Zuo, W., Hu, J., and Chen, Q. 2010. "Improvements on FFD modeling by using different numerical schemes," *Numerical Heat Transfer, Part B: Fundamentals*, 58(1), 1-16.

# Improvements on FFD Modeling by Using Different Numerical Schemes

Wangda Zuo, Jianjun Hu, Qingyan Chen
National Air Transportation Center of Excellence for Research in the Intermodal Transport Environment (RITE), School of Mechanical Engineering, Purdue University, 585 Purdue Mall, West Lafayette, IN 47907-2088USA
Qingyan Chen (Corresponding Author)
Email: yanchen@purdue.edu
Phone: +1-765-496-7562
Fax: +1-765-494-0539

## Abbreviated Title: Improvements on FFD Modeling

## Abstract
Indoor environment design and air management in buildings requires a fast simulation of air distribution. A Fast Fluid Dynamics (FFD) model seems very promising. This investigation was to develop the FFD by improving its speed and accuracy. The enhancement of computing speed can be realized by modifying the time-splitting method. The improvements on accuracy were done through replacing the finite difference scheme to the finite volume and through proposing a correction function for mass conservation. By using the new FFD model for different indoor airflows, the results show significant reduction on computing time and great improvements on accuracy.

Key Words: Fast Fluid Dynamics (FFD), Indoor Airflow Simulation, Time-Splitting Method, Finite Difference Method, Finite Volume Method

## NOMENCLATURE
**Roman Symbols**

| | |
|---|---|
| $f_i$ | body force(kg /m$^2$ s$^2$) |
| $H$ | room width, half channel height (m) |
| $k_T$ | thermal diffusivity (m$^2$/s) |
| $L$ | length scale (m) |
| $M$ | total mass flow rate (kg/s) |
| $P$ | pressure (kg/m·s$^2$) |
| $S_T$ | temperature source (K/s) |
| $T$ | temperature (K) |
| $t$ | time (s) |
| $U_i$, $U_j$ | velocity components in $x_i$ and $x_j$ directions, respectively (m/s) |
| $U$ | horizontal velocity component or velocity scale (m/s) |
| $V$ | vertical velocity component (m/s) |
| $x_i$, $x_j$ | spatial coordinates in i and j directions, respectively (m) |
| $x$, $y$ | spatial coordinates (m) |
| $\Delta t$ | time step (s) |

**Greek Symbols**

| | |
|---|---|
| $\alpha$ | ratio of mass flow rate to a flow domain over that out of the flow domain |
| $\rho$ | fluid density (kg/m$^3$) |
| $\nu$ | kinematic viscosity (m$^2$/s) |

## 1. Introduction
Building engineers often demand a fast solution of airflow in and around buildings so that they can provide different alternatives when they interact with architects for designing built environment. The fast simulation of airflow is also very important for air management, such as managing airflow in buildings in case of fire. The most popular models for predicting indoor air distributions are multizone network models, zonal models, and Computational Fluid Dynamics (CFD) models [1].

Multizone network models assume that indoor air is well-mixed in a zone (usually a room), so it needs only one computing node to represent the air property in that zone [2]. Thus, the multizone

network model can calculate the air distribution in a moderate size building with a few hundreds of nodes. As a result, the simulation time of the multizone network models can be as short as a few seconds. The multizone network models have been applied for the quick simulation of contaminant transportation in a whole building [3] and for the control of outdoor air supply to reduce energy consumption [4]. However, the well-mixed assumption in the multizone network models is not proper for an indoor space with temperature stratification, such as a large space, a room with displacement ventilation, or a room with natural ventilation [5].

Zonal models [6] further divide a room into several small subzones according to known flow pattern, which can be measured or estimated in advance. Researchers have employed zonal models to predict thermal performance of a whole building [7] andto investigate indoor air quality [8]. However, applications of the zonal models are limited since the model parameters depend on prior knowledge of indoor air distributions, which may not always be available.

To study indoor air distributions with high accuracy, the CFD has been the most popular approach at present [1, 9]. By solving the Navier-Stokes equations and other conservation equations for mass, energy, and species, the CFD can provide the most detailed information of indoor air distributions, such as air velocity, temperature, and contaminant concentration. The CFD has been used for analyzing indoor environment [10-12], designing ventilation systems [13-15] and for evaluating indoor air quality [16-18]. Furthermore, the CFD has been applied for studying smoke transport [19-21]. However, these studies were not for smoke management because they were too slow. In addition, the CFD can also be coupled with other building simulation models to improve their accuracy, such as with a multizone model [5] and with a building energy simulation program [22]. Unfortunately, the CFD simulations need very long computing time. Depending on CFD models, the computing time for a single space may range from a few hours to a few months. Obviously, the CFD models are not suitable for conceptual design of buildings and smoke management in case of building fire.

In order to simulate indoor air distributions with reasonable accuracy within an acceptable computing time, it is essential to find a model that is faster than the CFD and more accurate than the multizone and zonal models. Fast Fluid Dynamics (FFD) model fits the need. The FFD model was initiated for computer games [23]. The FFD model solves the Navier-Stokes equations in a way different from a CFD model. By sacrificing some accuracy, the FFD model can significantly reduce computing efforts. Although it was not as accurate as a CFD model, the FFD model could capture main flow features of indoor airflows and provide much more detailed information than the multizone and nodal models [24]. Most importantly, the computing speed of the FFD model was about 50 times faster than the CFD [24]. As an intermediate model between the multizone/nodal models and the CFD models, the FFD model could quickly predict the indoor air distribution for the conceptual design and emergency management.

However, the FFD model needs further improvements in order to be used for practice, which often deals with a building with many rooms and complex air distributions. The improvements include both computing speed and accuracy. For example, by running the FFD model on a graphics processing unit, the FFD simulation can be accelerated by 30 times [25]. In that work, the speed enhancement was achieved by using different computing hardware. This paper

reported our effort on improving numerical schemes for higher accuracy and for reducing the computing time.

## 2. Fast Fluid Dynamics Model

The FFD model developed by Stam [23] solves the Navier-Stokes equations:

$$\frac{\partial U_i}{\partial t} = -U_j \frac{\partial U_i}{\partial x_j} + \nu \frac{\partial^2 U_i}{\partial x_j^2} - \frac{1}{\rho}\frac{\partial P}{\partial x_i} + \frac{f_i}{\rho}, \tag{1}$$

where $U_i$ and $U_j$ are fluid velocity components in $x_i$ and $x_j$ directions, respectively; $\nu$ is kinematic viscosity; $\rho$ is fluid density; $P$ is pressure; t is time; and $f_i$ are forces, such as buoyancy force and other external forces. By using a first order time splitting method, the Eq. (1) can be split into four simple equations:

Source:

$$\frac{\partial U_i}{\partial t} = \frac{f_i}{\rho} \tag{2}$$

Diffusion:

$$\frac{\partial U_i}{\partial t} = \nu \frac{\partial^2 U_i}{\partial x_j^2} \tag{3}$$

Advection:

$$\frac{\partial U_i}{\partial t} = -U_j \frac{\partial U_i}{\partial x_j} \tag{4}$$

Projection:

$$\frac{\partial U_i}{\partial t} = -\frac{1}{\rho}\frac{\partial P}{\partial x_i} \tag{5}$$

The FFD scheme from Stam [23] solved Eqs. (2) and (3) with a first order implicit scheme. Then it employed a first order semi-Lagrangian method [26] for Eq. (4). To ensure mass conservation, Eq. (5) and continuity equation (Eq. (6)) were solved together using a pressure-correction projection method [27, 28].

$$\frac{\partial U_i}{\partial x_i} = 0 \tag{6}$$

If the flow involves heat transfer, the FFD method could solve the following energy equation:

$$\frac{\partial T}{\partial t} = -U_j \frac{\partial T}{\partial x_j} + k_T \frac{\partial^2 T}{\partial x_j^2} + S_T \tag{7}$$

where $T$ is temperature, $k_T$ is thermal diffusivity, and $S_T$ is heat source. The FFD scheme solved Eq. (7) in a similar way for Eq. (1) except the projection step.

The FFD scheme in our previous work computed the advection Eq. (4) after the diffusion Eq. (3). To solve the advection Eq. (4) with the semi-Lagrangian method, we need to trace a particle back to its location at the previous time step. This requires that the flow velocity field is divergence-free, which can be ensured by the continuity Eq. (6) in the projection step. Thus, our

previous work had an additional projection step before the advection step, so the implemented procedure in our previous program was:

Source → Diffusion → Projection → Advection → Projection (8)

One projection counts for about 23% of floating point operations of our FFD program. Thus, eliminating the additional projection step can greatly reduce the computing efforts. Nevertheless, the new scheme should not have significant negative influence on the current one.

In addition, our previous study [24] showed that the FFD was not as accurate as the CFD. One reason is that the FFD simulation results did not strictly satisfy mass conservation, as did the CFD. As a result, the unbalanced mass flow could introduce a significant number of errors to the simulation results. Thus, it is possible to improve the accuracy of the FFD simulation by enforcing the mass conservation.

## 3. Improvements on the FFD Scheme

Our effort to reduce the computing time was by eliminating the extra projection step in splitting method and to enhance the accuracy by enforcing the mass conservation.

### 3.1 Splitting schemes

The time splitting scheme allows one to compute the split equations in an arbitrary order [29]. Therefore, one can solve the advection equation in the beginning of each time step so that it is possible to eliminate the extra projection step. To further simplify the FFD scheme, one can also merge the source equation into the diffusion equation:

$$\frac{\partial U_i}{\partial t} = \nu \frac{\partial^2 U_i}{\partial x_j^2} + \frac{f_i}{\rho} \tag{9}$$

As a whole, the modified procedure of the FFD model is as follows:

Advection → Diffusion + Source → Projection (10)

### 3.2 Mass conservation

The FFD model is not as accurate as the CFD model. One possible reason is that the FFD cannot strictly satisfy the mass conservation. Many factors can cause the mass unbalance in the FFD simulation results, such as discretization methods, semi-Lagrangian approach and solver for the Poisson equation of pressure. To improve the mass conservation, our investigation replaced the finite difference scheme by the finite volume scheme. Since the finite volume method can naturally guarantee the mass conservation, it is widely used in flow simulation [30-34]. In addition, the following equation was further used to correct the velocity at the outlet:

$$U_{perp}^{new}\Big|_{out} = \left[1+\alpha\left(\frac{M_{in}}{M_{out}}-1\right)\right] U_{perp}\Big|_{out}, \tag{11}$$

where $M_{in}$ and $M_{out}$ are total mass flows into and out of the domain, respectively, $\alpha$ is a correction coefficient, $U_{perp}\Big|_{out}$ and $U_{perp}^{new}\Big|_{out}$ are the velocities perpendicular to the outlet surface before and after the correction. If a prefect mass balance is desired after the correction, $\alpha$ should be equal to 1.0. However, our study shows that $\alpha = 1.0$ will make the solution unstable. According to our experience, the optimized value of $\alpha$ should be around 0.7, which allows the program to reduce the mass imbalance quickly and stably.

Our study tested the impact of the proposed improvements one by one as listed on Table 1. FFD1 was used in our previous study [24]. FFD2 applied the modified time splitting method. Its implementation was also optimized to achieve a high performance in computing speed. Based on the FFD2, FFD3 employed the finite volume method. FFD4 further added the correction function for mass conservation (Eq. (11)).

## 4. Results

This section reports the performance of the improved numerical schemes by applying them for four different flows: a laminar flow in a lid-driven square cavity, a fully developed laminar flow in a plane channel, a turbulent flow with forced convection in an empty room, and a turbulent flow with mixed convection in an empty room.

### 4.1 Flow in a lid-driven cavity

The flow in a square lid-driven cavity as shown in Figure 1 was selected since the flow pattern looked like air circulation in a room. Based on the cavity height, $L$, and lid velocity, $U_0$, the Reynolds number of the flow studied was 100. This investigation employed four different meshes (17 × 17, 33 × 33, 65 × 65, and 129 × 129) to examine the grid independence and found 65 × 65 grids to be sufficiently fine. The reference was benchmark data from Ghia et al [35].

Figure 2 compares simulated air velocities at two mid cross-sections. All the FFD schemes provided the same results and also agreed with the reference data. This agreement indicates that the schemes do not affect the accuracy of the FFD simulations for the flow in the lid-driven cavity. Since the schemes were mainly proposed for solving problems in mass conservation in a domain with inlets and outlets, the flow in the lid-driven cavity did not fit into that category.

To evaluate the impact of different schemes on computing speed, we measured their computing time for a physical period of 10 s by using a time step of 0.01s with a grid resolution of 65 × 65. As shown in Table 2, the FFD2 code required half the computing time compared to that of the FFD1. The speed enhancement was for two major reasons: elimination of the extra projection and optimization of the implementation.

Table 2 also shows that the computing time used by the FFD2, FFD3 and FFD4 was similar. Thus, to change the discretization scheme (FFD3) and to add a correction for the mass conversation (FFD4) did not increase the computing load.

### 4.2 Flow in a plane channel

The feature of flow in a plane channel is similar to that in a corridor of a building. Based on the inlet velocity, $U_{in}$, and channel height, $2H$, the Reynolds number of simulated flow is 20. When the flow is fully developed, the velocity profile is parabolic and a theoretic solution is available:

$$U(y) = 3U_{in}\left(y - \frac{1}{2}y^2\right), \tag{12}$$

where $y$ is the distance to the low wall.

Our study used three grids distributions (16 × 8, 32 × 16, and 64 × 32) to solve the flow. Figure 3 shows calculated results with the finest grids (64 × 32). Discretized by the finite volume scheme, the FFD3 and FFD4 computed exact parabolic profiles for horizontal velocity. However, the

FFD1 and FFD2, which were discretized by the finite difference scheme, could not provide the exact results. The under-predicted horizontal velocity indicates less mass flow for this case. The profile calculated by FFD2 was poorer than that by FFD1. This means that eliminating one projection step could have a negative impact on mass conservation for the channel flow since the projection is responsible for mass conservation. However, this can be compensated by switching the discretization scheme from the finite difference (FFD2) to the finite volume (FFD3).

### 4.3 Forced convection in an empty room

Mechanical ventilation is widely used in modern buildings. The airflow by mechanical ventilation is forced convection. Thus, the numerical schemes are further evaluated by using airflow in an empty room with forced convection as shown in Figure 4 with experimental data from Nielsen [36]. The height of the room was $H$ and the length $3H$. The inlet was located at the upper-left corner and outlet at the lower-right corner. The widths of inlet and outlet were $0.056H$ and $0.16H$, respectively. Based on the inlet velocity, 0.455m/s, and inlet width, the corresponding Reynolds number was 5000. Since the experimental data showed a two-dimensional flow pattern in the room, our simulations were performed on a two-dimensional domain. Our study used three different meshes ($60 \times 20$, $120 \times 40$, and $240 \times 80$) and it turned out that flow patterns with different meshes were similar. Our discussion here used the results with $60 \times 20$ grids.

Figure 5 shows the calculated velocity fields. Since the experiment measured the velocity only at four lines, this investigation used the airflow pattern calculated by CFD with RNG $k$-$\varepsilon$ model [37] was used as a reference. The CFD results agreed very well with the experimental data in the four lines [38, 39]. Figure 5 shows that FFD1 and FFD2 calculated two large recirculations while the CFD results show only one large recirculation. The results from FFD3 and FFD4 were similar to those from CFD. Clearly, the discretization method played a very important role here. The finite volume scheme (FFD3 and FFD4) had performed much better than the finite difference scheme (FFD1 and FFD2).

Figure 6 further compares the velocity at the four lines by the FFD3 and FFD4 with the measured data. The results by FFD1 and FFD2 were not compared because the global pattern had showed to be very poor. Thus, a detailed comparison was meaningless. Figure 6 (a) and (b) are for two vertical locations ($x = H$ and $2H$). Both FFD3 and FFD4 were able to capture the trend in velocity profiles. However, the FFD3 greatly over-predicted the velocity near the walls. The FFD4 also over-predicted the velocity, but not as much as did the FFD3. One possible reason for the discrepancy was by the simple no-slip wall treatment used in FFD. Figure 6 (c) and (d) are for two horizontal locations. The velocity computed by FFD3 was negative in $y = 0.028H$ line at $x = 3H$ (right wall) as shown in Figure 6(c). The negative velocity implied a flow entering into the room through the outlet, which is obviously wrong. FFD4 could correct this problem through the correction function for mass conservation, although results along the line were not perfect.

### 4.4 Mixed convection in an empty room

The last case used to test different FFD schemes was a mechanically ventilated room with floor heating that generated a mixed convection flow. The flow pattern was influenced by both the inertial force and buoyancy force. The case was with experimental data from Blay et al [40]. Figure 7 shows the model room of 1.04 m × 1.04 m with supplied air at 15 $^{o}$C horizontally

injected into an empty room at a speed of 0.57 m/s. The temperature of the floor was 35.5 °C and that of the other walls at 15 °C. The measured data showed that the flow pattern was two-dimensional. Thus, the FFD simulations used two-dimensional meshes. Three different meshes (20 × 20, 60 × 60, and 120 × 120) were used and the results showed that the mesh with 60 × 60 was sufficiently fine.

Figure 8 demonstrates the flow pattern computed by the FFD with different numerical schemes. The experimental data [40] is used as reference. All the FFD schemes can correctly predict the large clock-wise recirculation in the center of the room, although there are some differences in the shape of the recirculation. The flow patterns calculated by the FFD3 and FFD4 were closer to the experimental data (Figure 8e) than those by the FFD1 and FFD2.

Both FFD1 and FFD2 predicted small secondary recirculations at the upper-left, upper-right, and lower-left corners. But the sizes of those secondary recirculation bubbles were larger than those in the reference data. The difference between the FFD1 and FFD2 was minor, so changing the splitting order and removing the extra projection function did not have a major impact on the overall flow pattern. This phenomenon is consistent with the finding in three previous cases.

The FFD3 computed a better airflow pattern than the FFD2. The FFD3 also captured two secondary recirculations at the upper-left and lower-left corners but not the one at the upper-right corner. In addition, the FFD3 predicted a lower velocity at the center of the room. By applying the correction function for mass conservation, the FFD4 can significantly improved the results when compared with FFD3. The overall flow field computed by FFD4 is very similar to the CFD data.

Figure 9 compares the velocity profiles at two mid cross-sections in the room ($x$ = 0.52 m and $y$ = 0.52 m). Surprisingly, the velocity profiles calculated by FFD1 and FFD2 at these two locations agree very well with the data except at the near wall regions. It could be coincidental in these two sections. The performance of FFD4 was not bad since its results were close to the experimental data.

Figure 10 further compares the simulated temperature profiles with the experimental data. The experimental data shows that air in the center of the room was well mixed and the air temperature was around 19 °C. All the four FFD simulations could capture the well-mixed phenomena in the center of the room since the computed temperatures were almost constant at the center. However, the FFD1 and FFD2 under-predicted the bulk temperature by 2 °C, while the FFD3 over-predicted it by 4 °C. Only FFD4 can properly compute the air temperature.

## 5. Conclusions

Our study presented in this paper was to further enhance the computing speed and accuracy of FFD for fast and informative simulation of airflow in buildings. A modified time-splitting method was used to eliminate the extra projection step. A finite volume discretization scheme was adopted to replace the finite difference scheme and a check on the mass balance between inlet and outlet was applied to enforce mass conservation for a better accuracy. This investigation examined the effectiveness of each measure by studying their performance step by step. The study led to the following conclusions:

(1) The modified time-splitting method can significantly reduce the computing time,

although it has a minor negative effect on the accuracy.

(2) To replace the discretization scheme from finite difference to finite volume can provide a little better accuracy.

(3) The correction function for mass conservation between inlet and outlet can evidentially improve the accuracy.

**Acknowledgements**

This study was funded by the US Federal Aviation Administration (FAA) Office of Aerospace Medicine through the National Air Transportation Center of Excellence for Research in the Intermodal Transport Environment under Cooperative Agreement 07-CRITE-PU. Although the FAA has sponsored this project, it neither endorses nor rejects the findings of this research. The presentation of this information is in the interest of invoking technical community comment on the results and conclusions of the research.

**REFERENCES**

1. Q. Chen, Ventilation Performance Prediction for Buildings: A Method Overview and Recent Applications, *Building and Environment*, vol. 44, pp. 848-858, 2009.

2. J. Axley, Multizone Airflow Modeling in Buildings: History and Theory, *HVAC&R Research*, vol. 13, pp. 907-928, 2007.

3. B. Hu, J. Freihaut, W. Bahnfleth, P. Aumpansub, and B. Thran, Modeling Particle Dispersion under Human Activity Disturbance in a Multizone Indoor Environment, *J. Architectural Engineering*, vol. 13, pp. 187-193, 2007.

4. X. Jin, H. Ren, and X. Xiao, Prediction-Based Online Optimal Control of Outdoor Air of Multi-Zone VAV Air Conditioning Systems, *Energy and Buildings*, vol. 37, pp. 939-944, 2005.

5. L. Wang, Coupling of Multizone and CFD Programs for Building Airflow and Contaminant Transport Simulations, Ph.D. thesis, Purdue University, West Lafayette, Indiana, 2007.

6. A. C. Megri and F. Haghighat, Zonal Modeling for Simulating Indoor Environment of Buildings: Review, Recent Developments, and Applications, *HVAC&R Research*, vol. 13, pp. 887-905, 2007.

7. C. Luo, B. Moghtaderi, H. Sugo, and A. Page, A New Stable Finite Volume Method for Predicting Thermal Performance of a Whole Building, *Building and Environment*, vol. 43, pp. 37-43, 2008.

8. F. Song, B. Zhao, X. Yang, Y. Jiang, V. Gopal, G. Dobbs, and M. Sahm , New Approach on Zonal Modeling of Indoor Environment with Mechanical Ventilation, *Building and Environment*, vol. 43, pp. 278-286, 2008.

9. P. V. Nielsen, Computational Fluid Dynamics and Room Air Movement, *Indoor Air*, vol. 14, pp. 134-143, 2004.

10. W. Zhang and Q. Chen, Large Eddy Simulation of Natural and Mixed Convection Airflow Indoors with Two Simple Filtered Dynamic Subgrid Scale Models, *Numer. Heat Transfer A*, vol. 37, pp. 447-463, 2000.

11. X. Li, B. Zhao, P. Guan, and H. Ren, Air Supply Opening Model of Ceiling Diffusers for Numerical Simulation of Indoor Air Distribution under Actual Connected Conditions, Part Ii: Application of the Model, *Numer. Heat Transfer A*, vol. 49, pp. 821-830, 2006.

12. V. C. Mariani and A. da Silva, Natural Convection: Analysis of Partially Open Enclosures with an Internal Heated Source, *Numer. Heat Transfer A*, vol. 52, pp. 595-619, 2007.

13. O. S. Asfour and M. B. Gadi, A Comparison between CFD and Network Models for Predicting Wind-Driven Ventilation in Buildings, *Building and Environment*, vol. 42, pp.

4079-4085, 2007.
14. T. Norton and D. W. Sun, Computational Fluid Dynamics (CFD) - an Effective and Efficient Design and Analysis Tool for the Food Industry: A Review, *Trends Food Sci. & Tech.*, vol. 17, pp. 600-620, 2006.
15. S. K. S. Boetcher and E. M. Sparrow , Numerical Simulation of Axisymmetric, Turbulent Buoyant Plumes - Application to Displacement Ventilation, *Numer. Heat Transfer A*, vol. 51, pp. 1023-1040, 2007.
16. R. Zhang, G. Tu, and J. Ling, Study on Biological Contaminant Control Strategies under Different Ventilation Models in Hospital Operating Room, *Building and Environment*, vol. 43, pp. 793-803, 2008.
17. B. Zhao and P. Guan, Modeling Particle Dispersion in Personalized Ventilated Room, *Building and Environment*, vol. 42, pp. 1099-1109, 2007.
18. B. Zhao, C. Yang, X. Yang, and S. Liu, Particle Dispersion and Deposition in Ventilated Rooms: Testing and Evaluation of Different Eulerian and Lagrangian Models, *Building and Environment*, vol. 43, pp. 388-397, 2008.
19. W. K. Chow and R. Yin, A New Model on Simulating Smoke Transport with Computational Fluid Dynamics, *Building and Environment*, vol. 39, pp. 611-620, 2004.
20. T. X. Qin, Y. C. Guo, C. K. Chan, and W. Y. Lin, Numerical Simulation of the Spread of Smoke in an Atrium under Fire Scenario, *Building and Environment*, vol. 44, pp. 56-65, 2009.
21. D. H. Chen, S. M. Lo, W. Z. Lu, K. K. Yuen, and Z. Fang, A Numerical Study of the Effect of Window Configuration on the External Heat and Smoke Spread in Building Fire, *Numer. Heat Transfer A*, vol. 40, pp. 821-839, 2001.
22. Z. Zhai and Q. Chen, Sensitivity Analysis and Application Guides for Integrated Building Energy and CFD Simulation, *Energy and Buildings*, vol. 38, pp. 1060-1068, 2006.
23. J. Stam. Stable Fluids, *Proc. of 26th International Conference on Computer Graphics and Interactive Techniques (SIGGRAPH'99)*, Los Angeles. 1999.
24. W. Zuo and Q. Chen, Real-Time or Faster-Than-Real-Time Simulation of Airflow in Buildings, *Indoor Air*, vol. 19, pp. 33-44, 2009.
25. W. Zuo and Q. Chen, Fast and Informative Flow Simulations in a Building by Using Fast Fluid Dynamics Model on Graphics Processing Unit *Building and Environment*, vol. 45, pp. 747-757, 2010.
26. R. Courant, E. Isaacson, and M. Rees, On the Solution of Nonlinear Hyperbolic Differential Equations by Finite Differences, *Communication on Pure and Applied Mathematics* vol. 5, pp. 243–255, 1952.
27. A. J. Chorin, A Numerical Method for Solving Incompressible Viscous Flow Problems, *J. of Comp. Phys.*, vol. 2, pp. 12-26, 1967.
28. Y. Y. Tsui and Y. F. Pan, A Pressure-Correction Method for Incompressible Flows Using Unstructured Meshes, *Numer. Heat Transfer B*, vol. 49, pp. 43-65, 2006.
29. H. Lomax, T. H. Pulliam, and D. W. Zingg, Fundamentals of Computational Fluid Dynamics, pp. 217-220, Springer, Berlin, New York, 2001.
30. E. O. B. Ogedengbe and G. F. Naterer, Convective Flux Dependence on Upstream Flow Directionality in Finite-Volume Computations, *Numer. Heat Transfer A*, vol. 51, pp. 617-633, 2007.
31. P. S. Glockner and G. F. Naterer, Numerical Simulation of Electrokinetic Flow and Heat Transfer in Microchannels with a Finite-Volume Method, *Numer. Heat Transfer A*, vol. 49, pp. 451-470, 2006.

32. M. Ko and N. K. Anand, Three-Dimensional Combined Convective-Radiative Heat Transfer over a Horizontal Backward-Facing Step - A Finite-Volume Method, *Numer. Heat Transfer A*, vol. 54, pp. 109-129, 2008.
33. K. Slimi, L. Zili-Ghedira, S. Ben Nasrallah, and A. A. Mohamad, A Transient Study of Coupled Natural Convection and Radiation in a Porous Vertical Channel Using the Finite-Volume Method, *Numer. Heat Transfer A*, vol. 45, pp. 451-478, 2004.
34. J. F. V. de Vasconcellos and C. R. Maliska, A Finite-Volume Method Based on Voronoi Discretization for Fluid Flow Problems, *Numer. Heat Transfer B*, vol. 45, pp. 319-342, 2004.
35. U. Ghia, K. N. Ghia, and C. T. Shin, High-Re Solutions for Incompressible Flow Using the Navier-Stokes Equations and a Multigrid Method, *J. of Com. Phys.*, vol. 48, pp. 387-411, 1982.
36. P. V. Nielsen, Specification of a Two-Dimensional Test Case, Aalborg University, Aalborg, Denmark, 1990.
37. V. Yakhot and S. A. Orszag, Renormalization-Group Analysis of Turbulence, *Phys. Rev. Lett.*, vol. 57, pp. 1722-1724, 1986.
38. Q. Chen, Comparison of Different K-E Models for Indoor Air-Flow Computations, *Numer. Heat Transfer B*, vol. 28, pp. 353-369, 1995.
39. W. Zhang and Q. Chen, Large Eddy Simulation of Indoor Airflow with a Filtered Dynamic Subgrid Scale Model, *Int. J. of Heat Mass Tranfer*, vol. 43, pp. 3219-3231, 2000.
40. D. Blay, S. Mergui, and C. Niculae, Confined Turbulent Mixed Convection in the Presence of Horizontal Buoyant Wall Jet, *Fundamentals of Mixed Convection*, vol. 213, pp. 65-72, 1992.

*Table 1 Improvements on the numerical schemes*

| Program | Splitting | Discretization | Correction for Mass Conservation |
|---|---|---|---|
| FFD1 | Eq. (8) | Finite Difference | No |
| FFD2 | Eq. (10) | Finite Difference | No |
| FFD3 | Eq. (10) | Finite Volume | No |
| FFD4 | Eq. (10) | Finite Volume | Yes |

*Table 2 Comparison of computing time used by different programs*

| Program | FFD1 | FFD2 | FFD3 | FFD4 |
|---|---|---|---|---|
| Computing Time (s) | 21.969 | 10.280 | 10.530 | 10.686 |

**Captions of Figures**

Figure 1. Schematic of the flow in a square lid-driven cavity.

Figure 2. Comparison of horizontal and vertical velocities in the lid-driven cavity predicted with different FFD schemes with the CFD data from Ghia et al [35].

Figure 3. Comparison of horizontal velocities calculated with different numerical schemes.

Figure 4. Schematic of an empty room with forced convection.

Figure 5. The airflow patterns calculated by the FFD with different numerical schemes and the CFD with RNG k-ε model.

Figure 6. Comparison of the velocity profiles in the empty room calculated by FFD with different numerical schemes.

Figure 7. Schematic of the airflow in a room with mixed convection.

Figure 8. Comparison of airflow pattern calculated by the FFD with different numerical schemes with the experimental data

Figure 9. Comparison of the air velocity profiles calculated by the FFD with different numerical schemes with the experimental data

Figure 10. Comparison of the air temperature profiles calculated by the FFD by using different numerical schemes with the experimental data from Blay et al. [40].

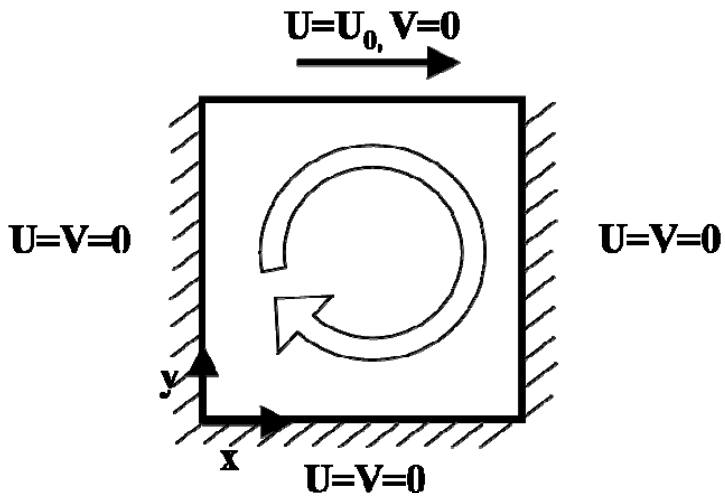

Figure 1

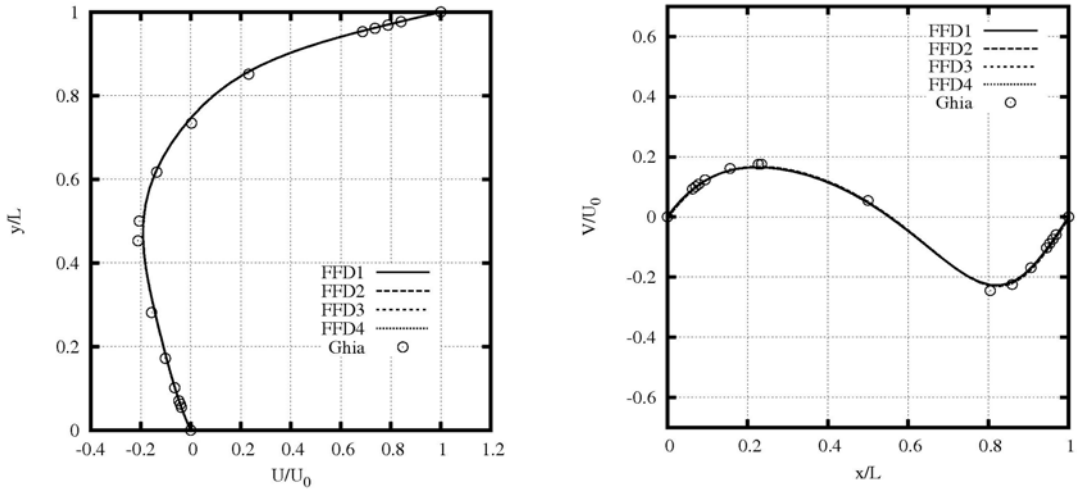


(a) U at x = 0.5L (b) V at y = 0.5L

Figure 2

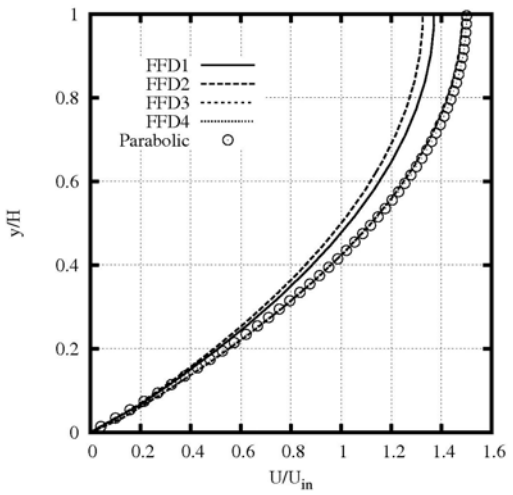


Figure 3

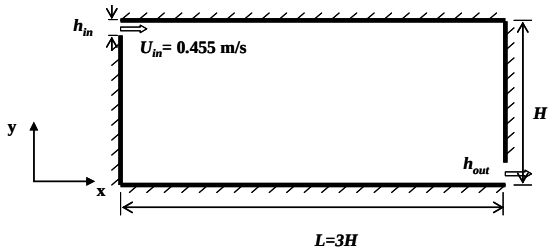

Figure 4

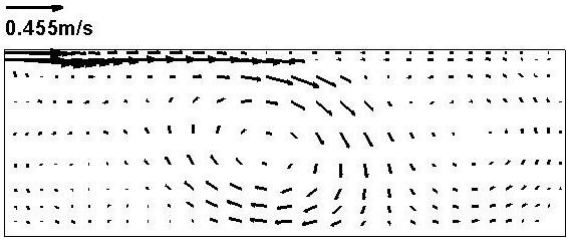


(a) FFD1

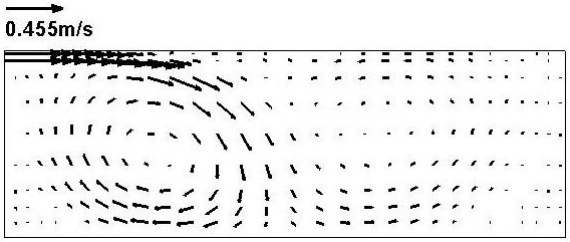


(b) FFD2

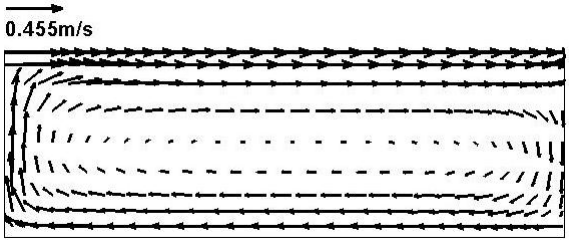


(c) FFD3

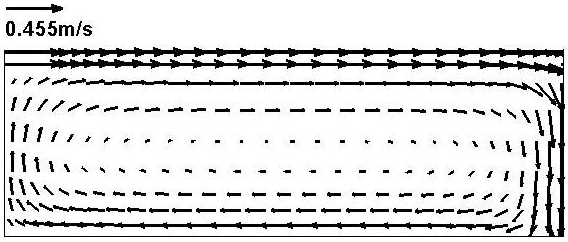


(d) FFD4

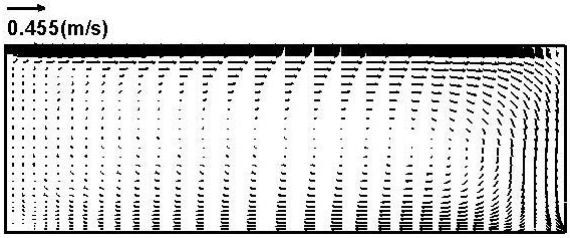


(e) CFD

Figure 5

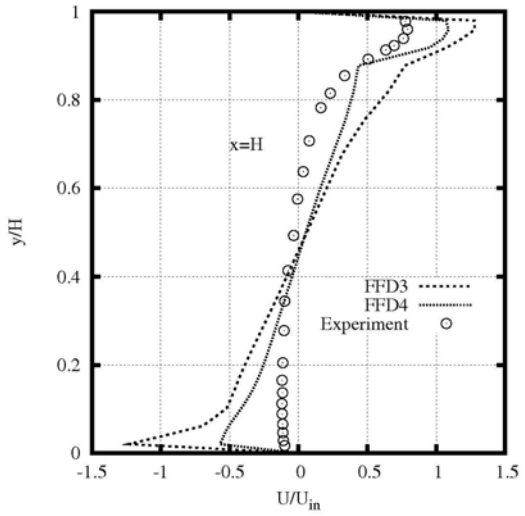


(a) x = H

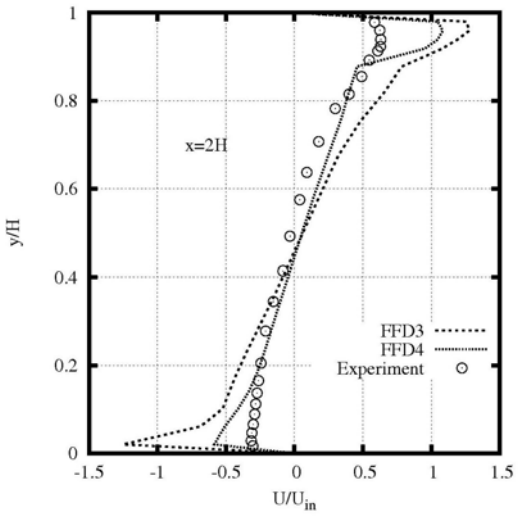


(b) x = 2H

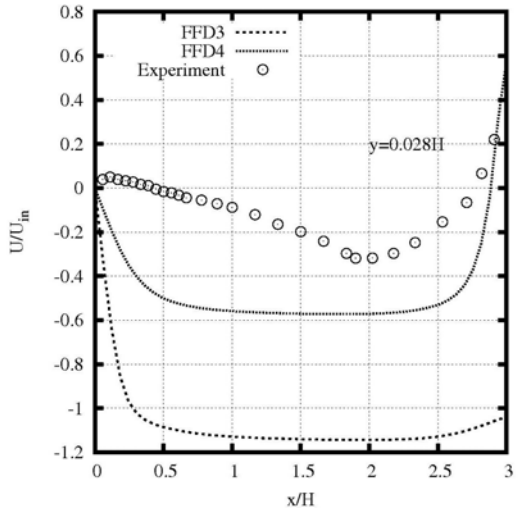


(c) y = 0.028H

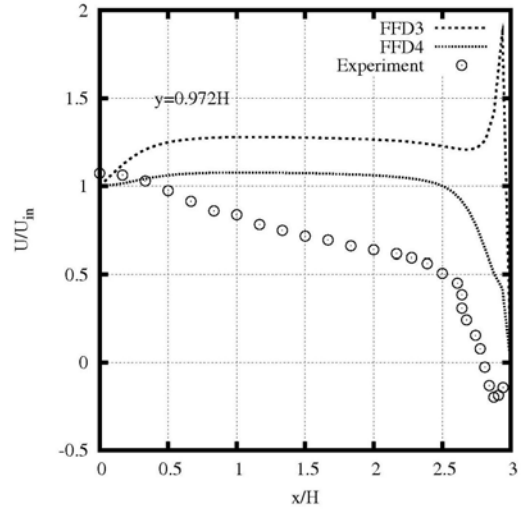


(d) y = 0.972H

Figure 6

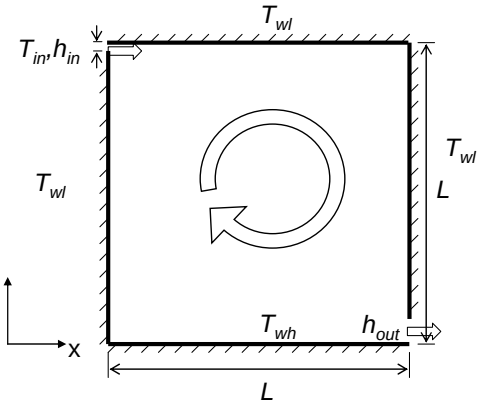

Figure 7

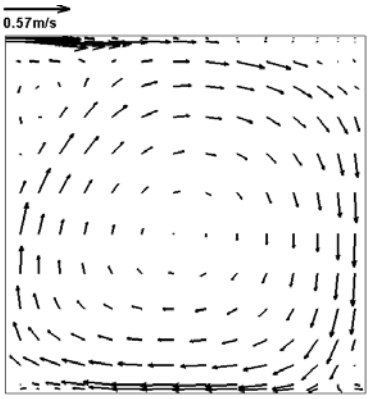


(a) FFD1

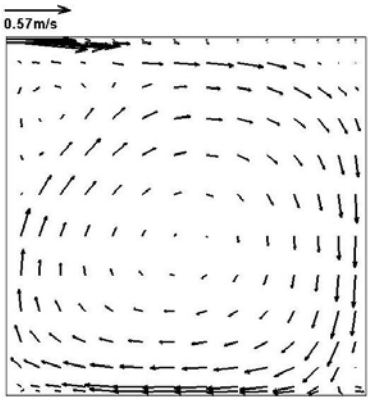


(b) FFD2

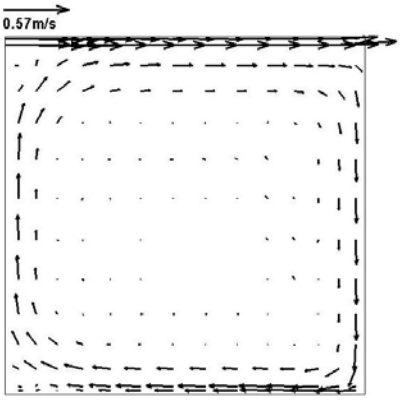


(c) FFD3

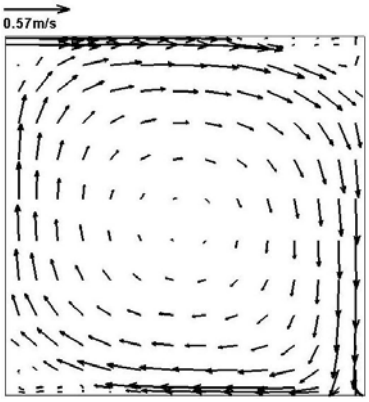


(d) FFD4

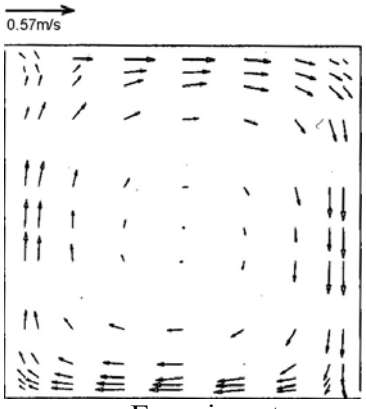


(e) Experiment

Figure 8

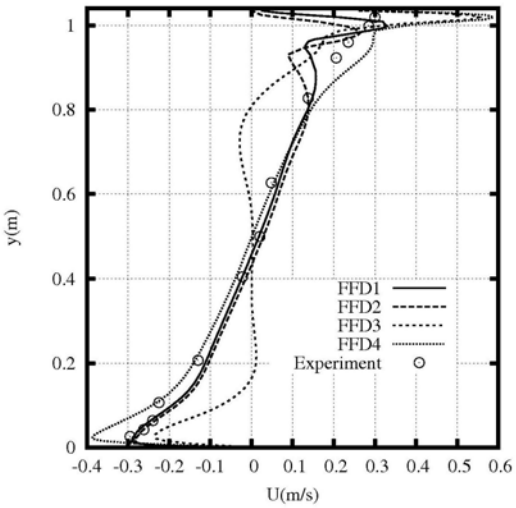


(a) U at x = 0.52m

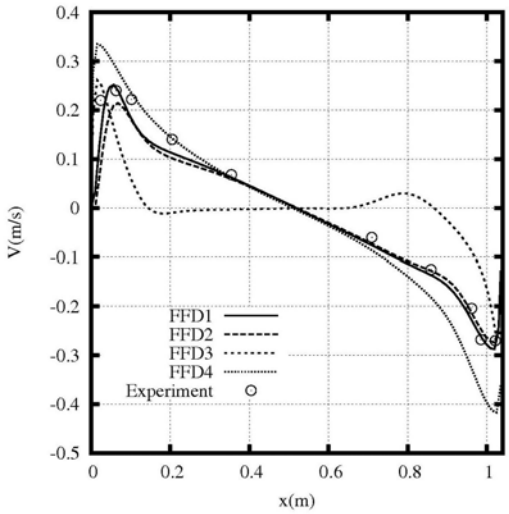


(b) V at y = 0.52m

Figure 9

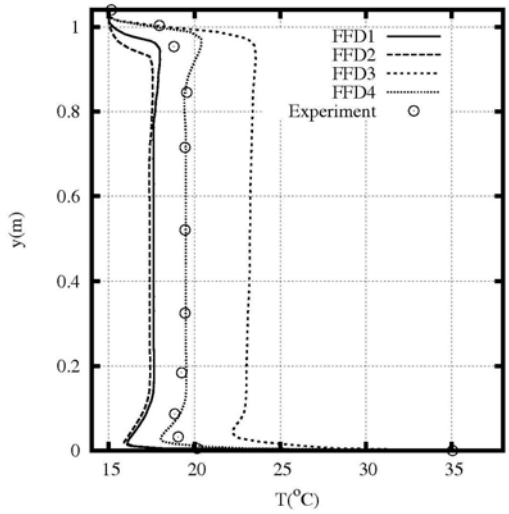


(a) T at x = 0.52m

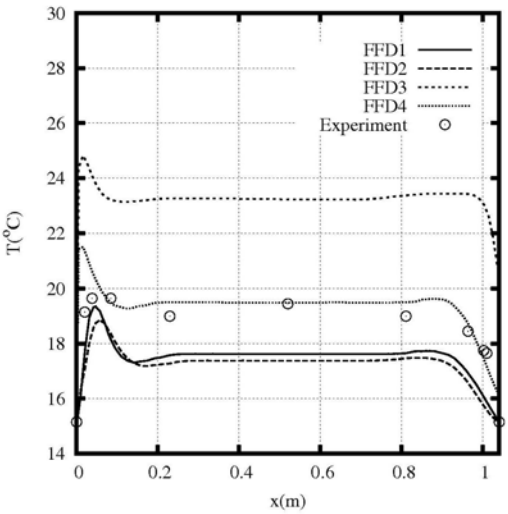


(b) T at y = 0.52m

Figure 10